Universiteit
Leiden
The Netherlands

On the geometry of fracture and frustration

Koning, V.

Citation
Koning, V. (2014, November 26). *On the geometry of fracture and frustration*. *Casimir PhD Series*. Retrieved from https://hdl.handle.net/1887/29873

Version:	Not Applicable (or Unknown)
License:	Leiden University Non-exclusive license
Downloaded from:	https://hdl.handle.net/1887/29873

Note: To cite this publication please use the final published version (if applicable).

Cover Page

Universiteit Leiden

The handle http://hdl.handle.net/1887/29873 holds various files of this Leiden University dissertation.

Author: Koning, Vinzenz
Title: On the geometry of fracture and frustration
Issue Date: 2014-11-26

Part I

SPHERICAL NEMATICS

We present a theoretical study of the director fields and energetics of spherical nematic liquid crystal shells with degenerate planar boundary conditions. There are divalent, trivalent and tetravalent shells with two, three and four defects at the outer boundary, respectively. For ultrathin trivalent shells, we find that the defects are optimally arranged in an isosceles triangle. We calculate the energy and the stability of this trivalent ground state, and compare this with the tetravalent and divalent defect configurations. For thick divalent shells with two pairs of surface defects, we investigate the effect of thickness inhomogeneity. The pairs of defects can undergo abrupt transitions from a configuration of maximum separation to a state in which the defects are confined to the thinner hemisphere. We construct a phase diagram that maps out the stability and coexistence of these two configurations as a function of shell thickness and thickness inhomogeneity. Our results compare favourably with the experimentally observed transitions in nematic double emulsion droplets and explain their hysteretic character.

2

THIN SHELLS

2.1 INTRODUCTION

One of today's major drives in condensed matter physics is the assembly of mesoscale particles into complex structures [29]. By creating anisotropy in the interparticle interactions, one can increase the complexity and functionality of these structures. A proposed way to achieve anisotropic interactions is by coating a spherical particle or droplet with an orientationally ordered phase [70]. The topology of the sphere enforces defects in the coating. Since these defects are very distinct regions on the sphere, they are suitable for the attachment of linkers acting as bonds between the particles. For instance, in the case of a vector order parameter, topology requires two defects, creating a particle with two binding sites. In fact, de Vries *et al.* have already assembled such divalent nanoparticle into chains [20]. Nematic rather than vector order allows for defects of charge one-half, referring to the 180 degrees rotation experienced by the local average orientation of the nematic molecules, $\mathbf{n}$, when encircling the defect. In fact, it is energetically favourable for defects of charge one to split into two charge one-half defects (Fig. 13a). Nematic order on the sphere has four topological defects of charge one half in its ground state, such that the sum of all charges is equal to 2, the Euler characteristic of the sphere, as demanded by the Poincare-Hopf theorem. Their mutual repulsion drives them as far away from each other as possible: at the vertices of a regular tetrahedron [57]. Thus, chemical functionalisation of the defects in the ground-state of two-dimensional nematic liquid crystal on the sphere would thus result in the diamond structure [70]. In section 3.2, however, we show the results of experimental investigations of nematic shells generated by trapping a water droplet inside a nematic droplet, revealing the existence of shells with valencies of two and three [24, 56, 41], besides the tetravalent shell. In the remainder of this chapter, we will focus on the defect separations (section 2.3), energetics (section 2.4) and fidelity of the

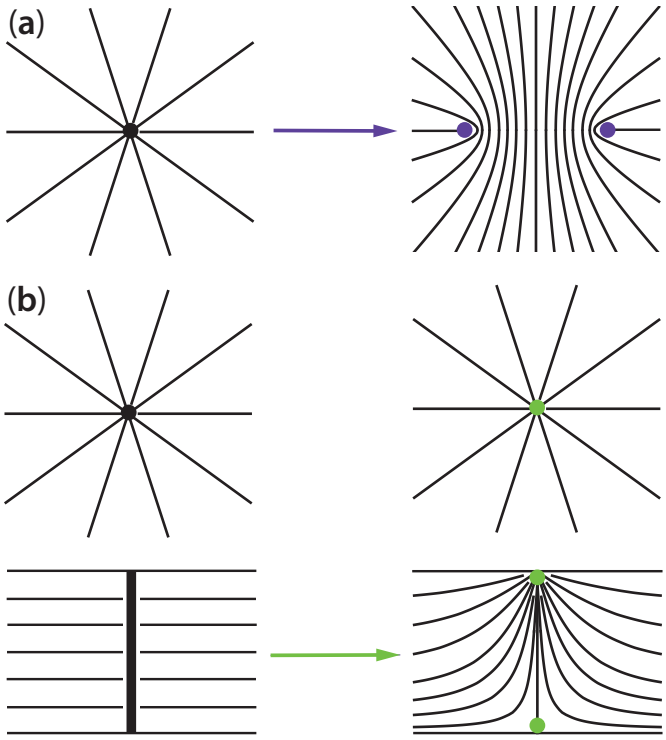

Figure 13: (a) In a two-dimensional nematic a $s = 1$ topological defect (black dot in left panel) can lower its elastic energy by splitting into two $s = 1/2$ defects (purple dots in right panel). (b) A singular line (left panel) spanning the shell with a winding number of one at the boundaries is topologically and energetically unstable. The singular core is indicated by a black dot in the top view shown in the top panel and by the vertical bold line in a cut shown in the bottom panel. One way of reducing the elastic energy escaping in the third (vertical) dimension (right panel), thereby leaving a point defect (green dot), called boojum, on each boundary.

bonds (section 2.5) in thin spherical nematic shells with three-fold valence. We will make a comparison with divalent and tetravalent shells and find the optimal valency as a function of shell thickness as well as the energy barrier between shells of different valency (section 2.4). We will conclude in section 2.6.

2.2 DIVALENT, TRIVALENT AND TETRAVALENT SHELLS

In this section we will present the experiments, performed by Teresa Lopez-Leon and Alberto Fernandez-Nieves, that corrobo-

rate our calculations in this chapter and chapter 3. To fabricate spherical nematic shells, one generates double emulsions with a microcapillary device [103]; these consist of a nematic drop that contains a smaller aqueous drop, all inside an aqueous continuous phase. Both the inner and outer water phases contain 1 wt% polyvinyl alcohol (PVA), which stabilises the emulsion against coalescence and enforces tangential anchoring of the rod-like molecules of the nematic liquid crystal, pentylcyanobiphenyl (5CB). The resulting double-emulsion drops are characterized by an outer radius, R, of around 50 μm and an inner radius, a, that are varied to produce shells of different average thicknesses, $h = R - a$, as schematically shown in Fig. 10. With this microfluidic method the thinnest shells that one can generate have $h \approx 1$ μm. However, it is possible to significantly reduce this value by increasing the volume of the inner drop once the double emulsion is formed. One achieves this by inducing a difference in osmotic pressure between the inner and outer water phases through the addition of a salt, $CaCl_2$. As pentylcyanobiphenyl has a finite permeability to water, an incoming flow of water from the outer phase can be established if the inner drop contains a higher salt concentration than the outer phase. By controlling this difference, one can control the kinetics of the process and ultimately the thickness of the shells.

Imaging the thinnest shells using optical microscopy and changing the focal plane of our microscope allows for precise determination of the position of the four defects; they are distributed throughout the shell, as shown by the images in Fig. 14a,b and by the schematic diagram in Fig. 14c. To obtain a meaningful value of the angular positions, one determines the position of all defects in a large number of shells with similar inner and outer drop sizes and plot the distribution for the central angle, θ_{ij}, which is the angle subtended by two defects (i and j) with respect to the centre of the drop, and the distribution for the surface angle, α, which is the angle subtended by two defects with respect to another defect. The resulting distributions are both Gaussian; they are centred at $\theta_{ij} = 109^\circ$ and $\alpha = 60^\circ$ and have a width of $\Delta\theta_{ij} = 20^\circ$ and $\Delta\alpha = 12^\circ$, as shown in Fig. 14d,e. The defects are thus located on the vertices of a regular tetrahedron.

There coexist divalent configurations (Fig. 15a,b) which, instead of four charge half defect lines spanning the shell, have two pairs of

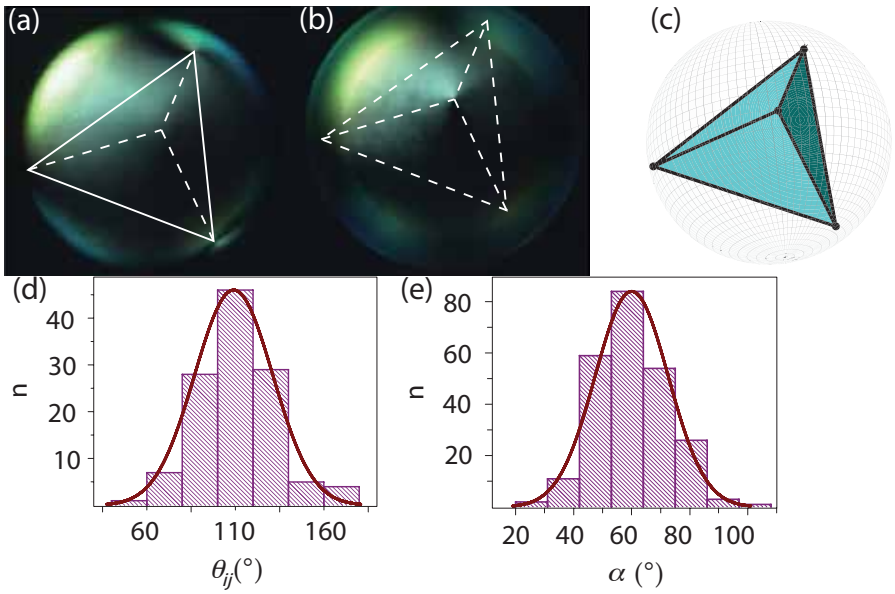

Figure 14: (a), (b) Cross-polarised images of a very thin shell with four $s = 1/2$ defects. In (a), two of the four defects are in focus, whereas in (b) we focus on the upper defect. (c) Schematic diagram of the observed arrangement of the four defects. (d), (e) Histograms for the central angle, θ_{ij}, and the surface angle, α, between defects. Ref. [56].

point defects, called boojums, residing on the boundary surfaces. They arise because the thickness of the nematic coating is nonzero: the elastic energy of a singular line with a winding number of one at the boundary is reduced by escaping in the third dimension, as is illustrated in Fig. 13b. This route thus forms an alternative to splitting into $s = 1/2$ lines spanning the shell. The defects maximise their distance and align, on average, along the diameter of the drop (Fig. 15a,b), as schematically shown in Fig. 15c, and by the central angle distribution in Fig. 15d.

Surprisingly, also structures containing both boojums as well as charge one-half disclination lines coexist (Fig. 16a-c). These defects structures have three-fold valence yet they are still consistent with Poincare-Hopf's theorem, because the total topological charge of the defects at the boundary is $1 + 1/2 + 1/2 = 2$, the Euler characteristic of the sphere. The three defects form an isosceles triangle, where the unequal angle originates from the single $s = 1$ defect, as schematically shown in Fig. 16d. The distribution for the two equal angles is centred at $\alpha_2 = 68°$ and has a width of $\Delta\alpha_2 = 15°$, as shown in Fig. 16e, whereas the distribution of the

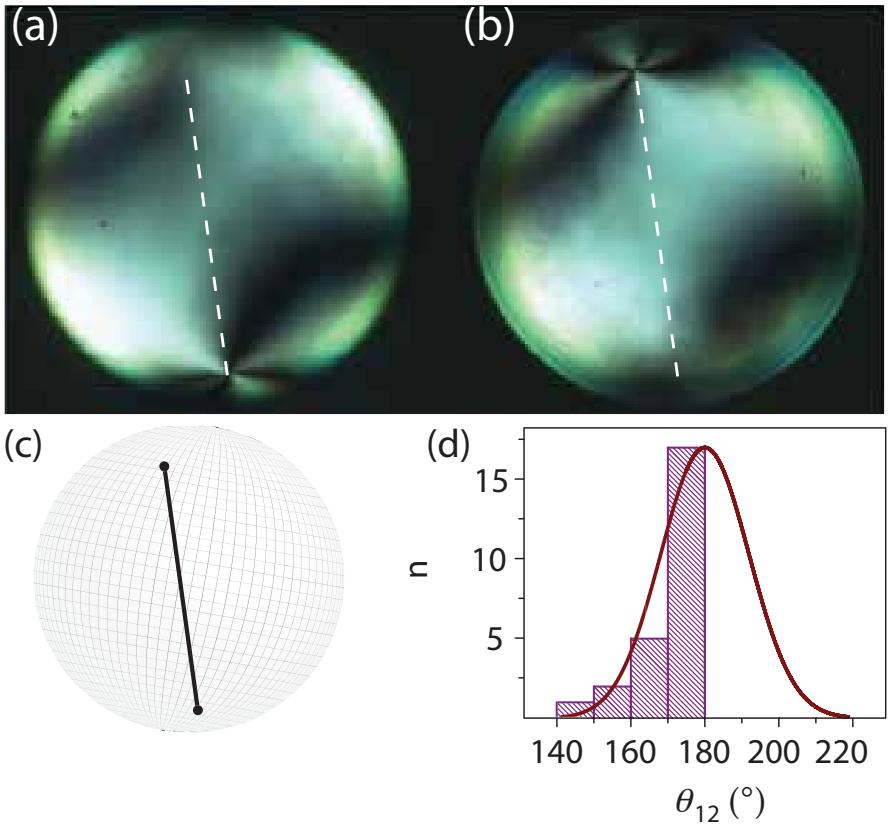

Figure 15: (a), (b) Cross-polarised images of a very thin shell with two $s = 1$ defects. (c) Schematic diagram of the observed arrangement of the two defects. (d) Histogram of the central angle, θ_{12}. Ref. [56].

unequal angle is centred at $\alpha_1 = 46°$ and has a width of $\Delta\alpha_1 = 12°$, as shown in Fig. 16f. Again, also this energetically stable defect configuration arises because of the thickness of the nematic coating is finite, and the energy barrier separating it from other defect structures will be reported in this chapter. The observed isosceles arrangement of the two $s = 1/2$ defects and the $s = 1$ defect is consistent with our calculation of the equilibrium configuration for these three defects on a spherical surface in the next section, which corresponds to $\alpha_1 = 66°$ and $\alpha_1 = 48°$.

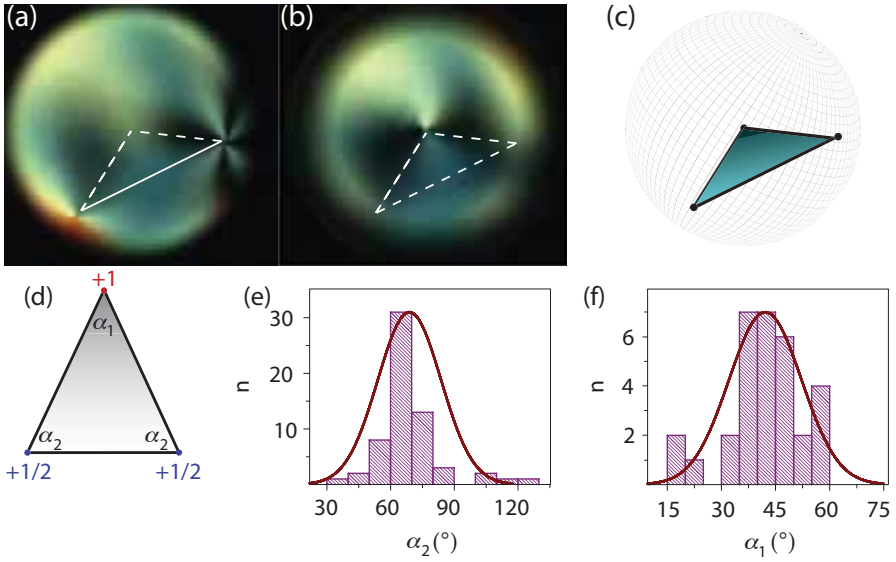

Figure 16: (a), (b) Cross-polarised images of a very thin shell with three defects, two $s = 1/2$ and an $s = 1$. In (a), one of the three defects is clearly in focus, with another defect slightly below this one. In (b) the third defect is in focus. (c) Schematic diagram of the three-dimensional arrangement of the three defects. (d) Isosceles triangle formed by the three defects, with α_1 the unequal surface angle. (e),(f) Histograms of the surface angles, α_1 and α_2. Ref. [56].

2.3 TRIVALENT GROUND STATE

The free energy of a thin curved nematic film (see section 1.4) reads

$$F = \frac{1}{2}\int dA \left[k_1 \left(D_i n^i\right)^2 + k_3 \left(D_i n_j - D_j n_i\right)\left(D^i n^j - D^j n^i\right)\right], \tag{80}$$

where k_1 and k_3 are the two-dimensional splay and bend elastic constants and where D_i is the covariant derivative. Eq. (80) can be recast in terms of defect separation rather than the director field $\mathbf{n}$. For a spherical nematic, the elastic energy in the one-constant approximation $k = k_1 = k_3$ reads (see eq. (78))

$$F = -\pi k \sum_{i<j}^{Z} s_i s_j \log\left(1 - \cos\theta_{ij}\right) + \sum_{i}^{Z} E_i\left(R\right), \tag{81}$$

where s_i is the topological charge of defect i, θ_{ij} is the angular distance between defects i and j, and Z is the number of defects or valence number. The self-energy $E_i(R)$ is given by

$$E_i(R) = \pi K s_i^2 \log\left(\frac{R}{a}\right) + E_c, \tag{82}$$

where R is the radius of the sphere and a is a small scale cut-off preventing a divergence of the energy. E_c represents a core energy, which depends on the details of the microscopic interactions. The self-energy is responsible for the splitting of $+1$ defect in an ideal two-dimensional nematic, because of its proportionality with s_i^2. The other term in eq. (81) describes the repulsion between like-charged defects. We wish to find the optimal location for the defects in a thin homogeneous shell given that $s_1 = 1$, $s_2 = \frac{1}{2}$ and $s_3 = \frac{1}{2}$. This requires minimising the interaction term of the free energy. We minimise the interaction energy with respect to three independent variables, namely θ_{12}, θ_{13} and the angle, C, subtended by the two curved triangular sides (circular arcs) meeting at the charge-one defect. If we apply the law of cosines on the sphere:

$$\cos\theta_{23} = \cos\theta_{12}\cos\theta_{13} + \sin\theta_{12}\sin\theta_{13}\cos C, \tag{83}$$

we can eliminate θ_{23} in favour of C in the free energy, and demand $\frac{\partial F}{\partial \theta_{12}} = \frac{\partial F}{\partial \theta_{13}} = \frac{\partial F}{\partial C} = 0$. From the latter equation, $\frac{\partial F}{\partial C} = 0$, we obtain $C = \pi$, implying that the defects lie on a great circle (see Figs. 17 and 18). There is always a circle that can be drawn through three points on a sphere; the maximal radius of this circle reflects the repulsive nature of the defects. With some straightforward algebra the other two equations, $\frac{\partial F}{\partial \theta_{12}}$ and $\frac{\partial F}{\partial \theta_{13}} = 0$, then lead to

$$\theta_{12} = \theta_{13} = \pi - \arccos\frac{2}{3} \approx 0.73\pi \approx 131.8^\circ, \tag{84}$$

$$\theta_{23} = 2\arccos\frac{2}{3} \approx 0.54\pi \approx 96.4^\circ. \tag{85}$$

We thus find that the defects are located at the vertices of an isosceles triangle rather than equilateral triangle, shown in Figs. 17 and 18. This less symmetric configuration arises because of the asymmetry in the magnitude of the charges of the defect: the two $+1/2$ defects repel each other less strongly than a charge one and charge one-half such that θ_{12} and θ_{13} are larger than θ_{23}. This is in marked contrast with the regular tetrahedral configuration in

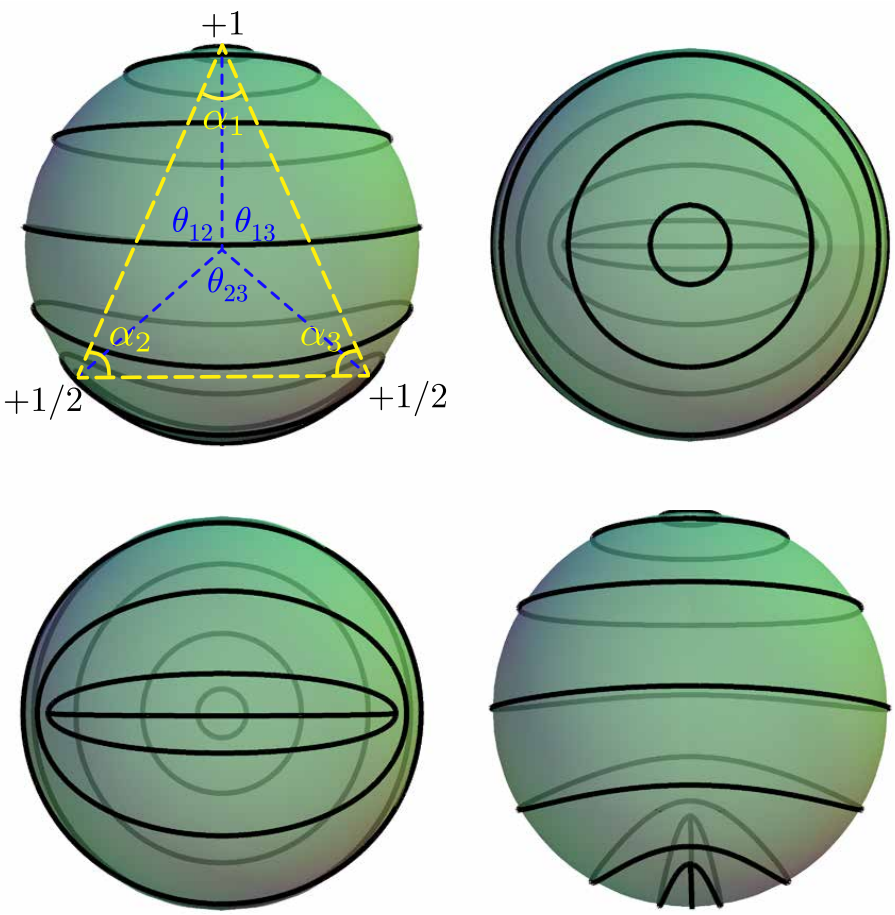

Figure 17: Four views on the bend texture of the director field on the sphere containing a +1 defect and two +1/2 defects arranged in an isosceles triangle with $\theta_{12} = \theta_{13} \approx 132°$, $\theta_{23} \approx 96.4°$, $\alpha_1 \approx 48°$ and $\alpha_2 = \alpha_3 \approx 66°$.

which all the defects are equidistant, because all four charges are indistinguishable. The fact that s_2 and s_3 are of equal magnitude is still reflected in the equal length of two of the sides ($\theta_{12} = \theta_{23}$) of triangle. Perhaps surprisingly, the distance between two charge one-half defects is smaller in the trivalent state than in the more 'crowded' tetravalent state. The surface angles of the flat triangle can be found be simple trigonometry: by realising that the triangle formed by two defects and the centre of the sphere is also an

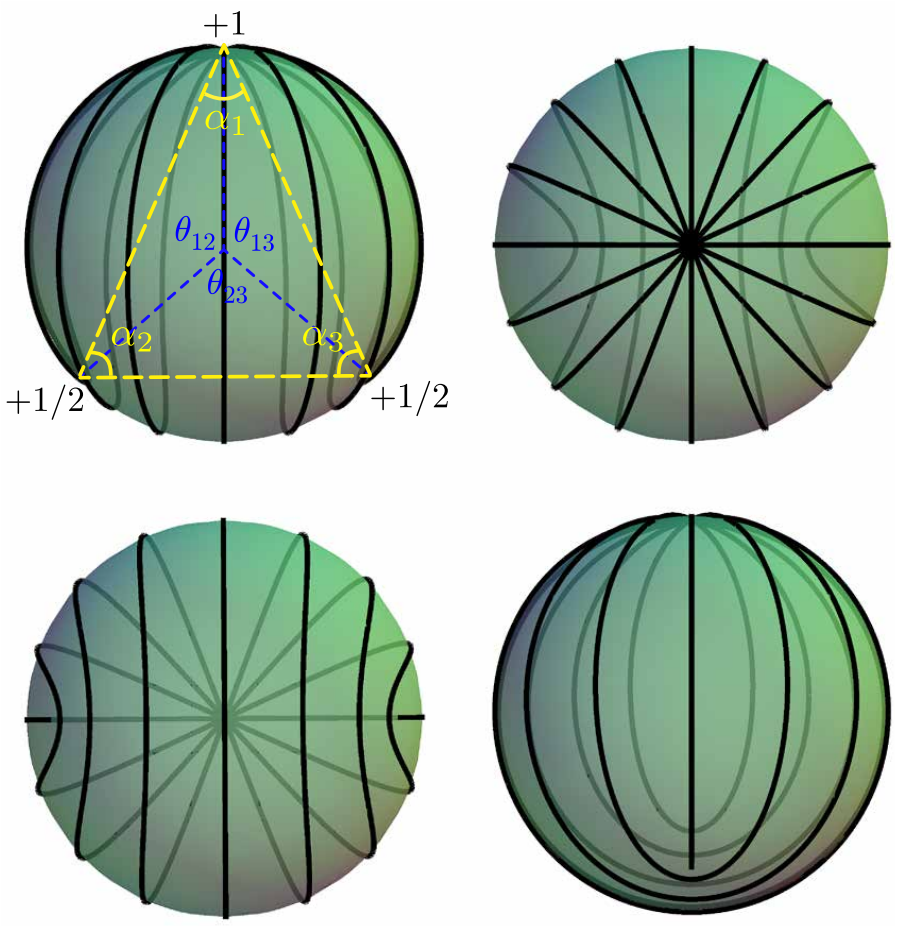

Figure 18: Four views on the splay texture of the director field on the sphere containing a +1 defect and two +1/2 defects arranged in an isosceles triangle with $\theta_{12} = \theta_{13} \approx 132°$, $\theta_{23} \approx 96.4°$, $\alpha_1 \approx 48°$ and $\alpha_2 = \alpha_3 \approx 66°$.

isosceles triangle (of which two sides have a length equal to the radius) we obtain

$$\alpha_1 = \pi - \theta_{12} = \arccos\frac{2}{3} \approx 48.2° \tag{86}$$

$$\alpha_2 = \alpha_3 = \frac{\theta_{12}}{2} = \frac{\pi}{2} - \frac{\arccos\frac{2}{3}}{2} \approx 65.9° \tag{87}$$

This is in close agreement with the experimental values reported in the previous section, which are are $\alpha_1 \approx 68°$ and $\alpha_2 \approx 46°$. Given the defect locations the energy-minimising director field can be found by means of a stereographic projection of the planar solution [57]. The bend texture is displayed in Fig. 18. Rotating this director field over an angle α yields the same free energy in the one-constant approximation. The splay texture (Fig. 17) corresponds

to $\alpha = \pi/2$. We note that the escape in the third dimension, in which singular region is distributed over a larger distance of the order of the thickness, occurs in shells of finite thickness and is somewhat different than the problem of three point defects in a two-dimensional nematic solved above. However, we expect that the defect separations will be marginally affected as long as the thickness is small compared to the radius.

2.4 VALENCE TRANSITIONS

We will now proceed with an estimate of the energy of the trivalent shell when this escape is taken into account. In doing so, we follow the arguments in ref. [105]. We first consider the energy when three singular lines are spanning the shell at angular distances reported above. We estimate this energy as the product of the two-dimensional result and the thickness, h, thus effectively taking $k = Kh$:

$$E'_{Z=3} = \pi Kh \left[\left(1 + 2 \times \frac{1}{4} \right) \log \left(\frac{R}{a} \right) - 0.54 + \frac{3E_c}{\pi Kh} \right]. \quad (88)$$

A heuristic yet adequate method to include the escape is to replacing the microscopic cut-off by the thickness of the shell, since the singular core is spread out over spatial dimensions of the order of h. To account for the pair of boojums an energy $4.2K\pi h$ is added [11, 105, 41]. We then obtain

$$E_{Z=3} = \pi Kh \left[\log \left(\frac{R}{h} \right) + \frac{1}{2} \log \left(\frac{R}{a} \right) + 3.65 + \frac{2E_c}{\pi Kh} \right]. \quad (89)$$

By comparing this to the energy of a shell with four disclination lines

$$E_{Z=4} = \pi Kh \left[\log \left(\frac{R}{a} \right) - 0.43 + \frac{4E_c}{\pi Kh} \right], \quad (90)$$

we can find the critical value for h above which the trivalent defect configuration is energetically preferable over the tetravalent one:

$$h^*_{34}/R = e^{4.08 - 2E_c/\pi Kh} \sqrt{\frac{a}{R}} \quad (91)$$

Similarly, one can find the critical value for h below which the trivalent defect configuration is energetically preferable over the divalent one by setting $E_{Z=3}$ equal to the approximation of the

energy of a shell with two diametrically opposite pairs of surface defects, $E_{Z=2}$. Again, we will first find the energy of a shell with two singular lines

$$E'_{Z=2} = \pi K h \left[2 \log \left(\frac{R}{a} \right) - 0.69 + \frac{2E_c}{\pi K h} \right], \tag{92}$$

after which we apply the same trick as we used to find $E_{Z=3}$ to obtain

$$E_{Z=2} = \pi K h \left[2 \log \left(\frac{R}{h} \right) + 7.69 \right]. \tag{93}$$

We find a very similar value

$$h^*_{23}/R = e^{4.04 - 2E_c/\pi K h} \sqrt{\frac{a}{R}}. \tag{94}$$

The energy as a function of thickness is plotted in Fig. 19 for all three different valencies. Since $h^*_{23} < h^*_{34}$ there is no h for

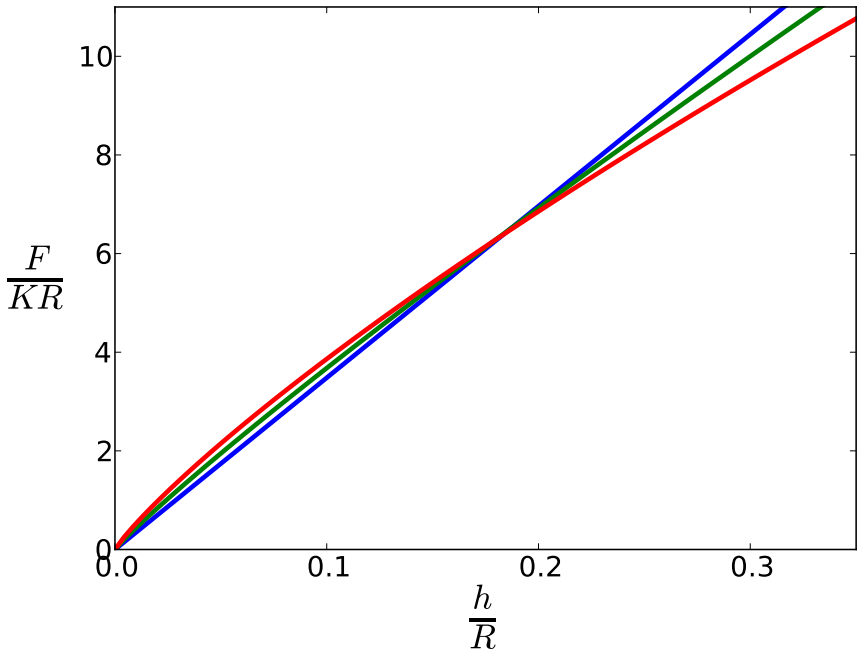

Figure 19: Elastic energy as a function of shell thickness for divalent (red), trivalent (green) and tetravalent (blue) defect configuration for $R/a = 10^5$ and $E_c = 0$. Either the divalent or tetravalent configuration, but not the trivalent configuration, is lowest in energy.

which the trivalent shell has lower energy than both the divalent and tetravalent shell. The energy barriers between them however

are very large. The energy barrier for going from the trivalent to tetravalent shell lies in undoing the escape and is thus the difference between $E'_{Z=3}$ and $E_{Z=3}$:

$$\Delta E_{3\to 4} = \pi K h \left(\log\left(\frac{h}{a}\right) - 4.19 + \frac{E_c}{\pi K h} \right). \tag{95}$$

The energy barrier for going from the trivalent to tetravalent shell lies in overcoming the repulsion between the two $+1/2$ defects and can thus be estimated by the difference between $E'_{Z=2}$ and $E'_{Z=3}$:

$$\Delta E_{3\to 2} = \pi K h \left(\frac{1}{2}\log\left(\frac{R}{a}\right) - 0.15 - \frac{E_c}{\pi K h} \right). \tag{96}$$

Since $K \approx 10^{-11} N$, for a thin shell with $h = 1\ \mu m$, these barriers are four orders of magnitude larger than the thermal energy scale (at room temperature), $k_B T$, where T denotes temperature and k_B is Boltzmann's constant, thus providing stability of the trivalent state. Valence transitions are unlikely to occur.

2.5 BOND FIDELITY

In this section, we will consider the fidelity of the three bonds by considering its robustness against thermal fluctuations. We will expand the energy around the equilibrium values for the zenith and azimuthal angles, $\{\theta_i^0, \phi_i^0\}$. We parametrise the departures from the equilibrium angles with a $2Z$-component vector $\mathbf{q}$, whose first three components are the deviations along the lines of longitude of the sphere and whose final three components are the deviations along the lines of latitude of the sphere. We thus have

$$q_i = \delta\theta_i, \tag{97}$$
$$q_{3+i} = \delta\phi_i \sin\theta_i. \tag{98}$$

Again we employ the law of cosine on the sphere:

$$\begin{aligned} \cos\theta_{ij} = &\cos\left(\theta_i^0 + q_i\right)\cos\left(\theta_j^0 + q_j\right) \\ &+ \sin\left(\theta_i^0 + q_i\right)\sin\left(\theta_j^0 + q_j\right) \\ &\times \cos\left(\phi_i^0 - \phi_j^0 + \frac{q_{3+i}}{\sin\theta_i^0} - \frac{q_{3+j}}{\sin\theta_j^0}\right), \end{aligned} \tag{99}$$

to rewrite F in eq. (81) as an expansion to quadratic order in q:

$$F = F\left(\theta_i^0, \phi_i^0\right) + \frac{1}{2}\sum_{ij} M_{ij} q_i q_j + \mathcal{O}\left(q^4\right). \tag{100}$$

The 6×6 matrix M can thus be found by

$$M_{ij} = \left(\frac{\partial^2 F}{\partial q_i \partial q_j}\right)_{q_i = q_j = 0}. \tag{101}$$

This calculation is performed without loss of generality upon choosing the ground state defect locations to be on the equator, *i.e.* $\theta_i^0 = \pi/2$. We diagonalise this matrix:

$$M = UDU^T. \tag{102}$$

The matrix D has the following eigenvalues on the diagonal:

$$\{\lambda_i\} = \frac{\pi k}{20}\{0, 0, 0, 15, 17, 18\}. \tag{103}$$

The columns of the matrix U are the corresponding orthonormal eigenvectors, $\{\mathbf{u}_i\}$, and U^T is the transpose of U. The eigenvectors belonging to the three zero eigenvalues represent rigid body rotations. The other eigenvectors are

$$\mathbf{u}_4 = \begin{pmatrix} 0 \\ 0 \\ 0 \\ 0 \\ -\frac{1}{\sqrt{2}} \\ \frac{1}{\sqrt{2}} \end{pmatrix}, \quad \mathbf{u}_5 = \begin{pmatrix} \frac{4}{\sqrt{34}} \\ \frac{3}{\sqrt{34}} \\ \frac{3}{\sqrt{34}} \\ 0 \\ 0 \\ 0 \end{pmatrix}, \quad \mathbf{u}_6 = \begin{pmatrix} 0 \\ 0 \\ 0 \\ \sqrt{\frac{2}{3}} \\ \frac{1}{\sqrt{6}} \\ \frac{1}{\sqrt{6}} \end{pmatrix}. \tag{104}$$

The fourth and sixth eigenvalues also correspond to deformations that keep the defects located at a great circle. The fourth one corresponds to a displacement of the charge one-half defects such that their distance to the charge one defect grows or shrinks in equal manner and hence preserves the isosceles shape of the triangle (Fig. 20a). The sixth eigenvalue corresponds to a mode of deformation that does not posses this property, thus breaking the symmetry of reflection across the bisector of the distinct angle (Fig. 20c). The mode of deformation corresponding to the fifth eigenvalue, however, retains the isosceles shape of the triangle, but shrinks the

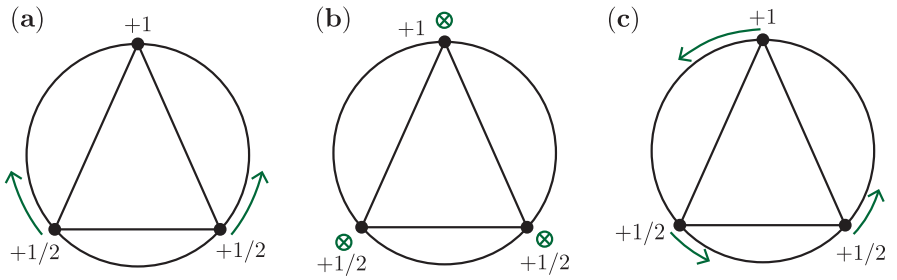

Figure 20: Schematics of the three non-trivial eigenmodes corresponding to (a) $\mathbf{u}_4$, (b) $\mathbf{u}_5$ and (c) $\mathbf{u}_6$. The defects (represented by dots) continue to lie on a great circle in (a) and (c), but not in (b). The defects continue to form an isosceles triangle in (a) and (b), but not in (c).

size of the triangle as the defects do not lie on a great circle anymore (Fig. 20b). We change the basis from q_i to w_i, which is the departure from the trivalent ground state in the i-th eigendirection:

$$q_i = U_{ij} w_j. \tag{105}$$

This basis transformation yields to quadratic order in w_i:

$$F = F\left(\theta_i^0, \phi_i^0\right) + \frac{1}{2}\lambda_4 w_4^2 + \lambda_5 w_5^2 + \lambda_6 w_6^2. \tag{106}$$

By equipartition, each term contributes $\frac{1}{2}k_B T$. The eigenvalues corresponding to the trivalent modes of deformation are equal or larger than the the tetravalent ones (which are $\frac{3}{8}\pi k$ and $\frac{3}{4}\pi k$ [70, 105]): the trivalent ground state is thus somewhat better protected against thermal fluctuations.

2.6 CONCLUSION

In a spherical nematic shell of finite thickness a stable defect structure with two $s = 1/2$ lines and one pair of boojums is observed experimentally, besides the bipolar and regular tetrahedral configuration. If the shell is thin and homogeneous in thickness, the repulsive interdefect interaction pushes the defects to lie on a great circle. The strength of the interaction depends on the charges of the defects. Consequently, the defects are located at the vertices of an isosceles triangle rather than an equilateral triangle, in contrast

to the tetravalent ground state in which the defects are equidistant. In the energetically most favourable trivalent configuration, we obtain for the central angles $\theta_{12} = \theta_{13} = 0.73\pi$, $\theta_{23} = 0.54\pi$ and for the angles in the (flat) isosceles triangle $\alpha_1 = 48°$ and $\alpha_2 = \alpha_3 = 66°$. These values are in good agreement with experimental values. Estimations of the elastic energy show that there is no shell thickness for which the trivalent ground state is lower than both the tetravalent and divalent ground state. However, there are large energy barriers to provide stability for the trivalent state once it is created.